PHYSICAL REVIEW B VOLUME 47, NUMBER 4 15 JANUARY 1993-II

Finite-size effects on the optical functions of silicon microcrystallites: A real-time spectroscopic ellipsometry study

Hien V. Nguyen and R. W. Collins
Materials Research Laboratory and the Department of Physics, Pennsylvania State University, University Park, Pennsylvania 16802
(Received 31 July 1992; revised manuscript received 28 September 1992)

We have performed real-time spectroscopic ellipsometry (SE) measurements over the photon-energy range from 1.5 to 4.0 eV during the growth of microcrystalline silicon (μc-Si:H) by plasma-enhanced chemical-vapor deposition on chromium at 250 °C. We focus on the regime when the film consists of isolated microcrystallites and intervening void volume. In this regime, the observed three-dimensional growth behavior allows us to associate the crystallite size with the physical thickness of the film. The SE measurements are self-contained in that they provide not only microstructural information, including film thickness and void-volume fraction, but also the effective optical functions of the film. From this combination of results, the optical functions of the Si crystallites, themselves, can be deduced by mathematically extracting the influence of the void-volume fraction on the effective optical functions. A critical-point (CP) analysis of the E_1 transitions visible near 3.3 eV in the crystallite optical functions provides information on the electronic properties as a continuous function of crystallite size. Over the physical thickness range accessible in these experiments (~200–250 Å), the transition energy and phase deduced in the CP analysis are constant at the single-crystal values, within experimental error, while the broadening parameter decreases with increasing thickness. The latter behavior is consistent with a finite-size effect in which electron scattering at surfaces modifies the optical response of the microcrystallites.

I. INTRODUCTION

The optical properties of microcrystalline silicon (μc-Si:H) prepared by plasma-enhanced chemical-vapor deposition are interesting, owing to applications of the material in a number of amorphous silicon (a-Si:H)-based multilayer devices.[1] For example, B-doped μc-Si:H has been applied as the top layer in photovoltaic devices because of its higher electrical conductivity and weaker optical absorption in comparison to doped a-Si:H.[2,3] Microcrystalline Si:H is also an interesting material from a fundamental standpoint, because it can serve as a model system for studying the effects of crystalline particle or grain size on the optical and electronic properties of semiconductor films.[4]

Previous research has shown that the near-ultraviolet optical functions of both polycrystalline silicon (p-Si) (Ref. 5) and μc-Si:H (Ref. 6) thin films can be simulated accurately with the Bruggeman effective-medium theory (EMT) using a model of the material as a three-component, microscopic composite consisting of a-Si, c-Si, and void. In such studies, spectroscopic ellipsometry (SE) data collected on the films are subjected to linear-regression analysis in order to extract the volume fractions of the two independent components as well as the thickness and composition of roughness and/or oxide overlayers.[7] To assess the statistical significance and overall quality of the fits, the procedure of Ref. 7 relies on the 90% confidence limits as well as the unbiased estimator of the mean-square deviation, computed between experimental and calculated values of the real and imaginary parts of the amplitude reflection coefficient ratio (p-to-s). Recently, however, this fitting procedure has been improved through use of the biased estimator, allowing one to weight more strongly the parts of the spectra with higher experimental accuracy.[8]

Although simulations of p-Si and μc-Si:H as three-component composites yield excellent fits to the measured ellipsometric spectra, attempts to correlate the resulting bulk-film structural information with that deduced from Raman spectroscopic analysis of the same samples have revealed an ambiguity in the SE interpretation.[9] Specifically, some films that exhibit a considerable volume fraction of a-Si from SE have shown no such detectable phase from Raman spectroscopy. This result suggests that the a-Si component in the SE analysis may serve the additional role of simulating the broadening of the optical transitions that arises from a reduction in the excited-state lifetime of electrons due to scattering from grain boundaries or defects within the grains. These effects are not included in the EMT, which employs the assumption that the optical functions of the c-Si component in p-Si and μc-Si:H films are identical to those of the single crystal.[7] More recent studies have qualitatively supported a finite-size-effect interpretation of the optical properties of these materials by drawing attention to a correlation between the measured grain size and the broadening parameter, the latter deduced from a critical-point analysis of the $E_0'-E_1$ optical transitions in the c-Si grains at room temperature.[10,11]

We have exploited new opportunities made possible by the recent development of real-time SE to study the optical properties of μc-Si:H in greater detail. Real-time SE is advantageous for two reasons. Obviously, the real-time

 ©1993 The American Physical Society

approach avoids artifacts due to oxidation or surface contamination from the ambient atmosphere. More importantly, because the raw ellipsometric spectra can be analyzed to extract the physical thickness of the film as well as its optical functions, measurements of the films in the isolated crystalline particle regime versus time prior to particle contact can provide information on the electronic structure (from the optical transitions) as a continuous function of the particle dimension (or physical thickness). Thus, the power of the measurement approach is matched by no other single, currently available technique.

II. EXPERIMENTAL DETAILS

The real-time spectroscopic ellipsometer used in this study consists of a Xe arc source, collimator, rotating polarizer, sample in vacuum chamber, analyzer, spectrograph, 1024-pixel silicon photodiode detector array, and detector controller, as described in greater detail elsewhere.[12,13] Using the detector controller, the array is grouped by eight to increase the signal-to-noise ratio, but at the expense of spectral resolution. Windows on the vacuum chamber provide optical access to the μc-Si:H film surface during growth. Real-time ellipsometric spectra in (ψ,Δ) are collected from 1.5 to 4.0 eV in 3.8 s as an average of 80 polarizer optical cycles. Here, (ψ,Δ) are defined, as usual, by $\tan\psi \exp(i\Delta) \equiv r_p/r_s$, where r_p and r_s are the complex amplitude reflection coefficients for p and s polarization states. The elapsed time between one measurement and the next is 21 s. This extended measurement cycle includes background correction, raw data reduction to (ψ,Δ), video display, and permanent storage.

The μc-Si:H thin films were prepared by plasma-enhanced chemical-vapor deposition (PECVD) in the parallel-plate configuration with the substrate mounted on the grounded anode, as first reported in Ref. 14. The following parameters were set: substrate temperature, 250 °C; SiH_4/H_2 gas-flow ratio, 1/80 in standard cm^3/min; total gas pressure, 0.4 Torr; net rf power, 20 W; and power flux at the film surface, 520 mW/cm^2. Under these conditions, the deposition rate is 16 Å/min, expressed in terms of physical thickness. At this rate, 1 Å accumulates during the (ψ,Δ) spectra measurement time, and spectra are collected every ~6 Å. The substrate was Corning 7059 glass, overcoated with an opaque layer of chromium, prepared by low-pressure magnetron sputtering for optimum smoothness and density. Chromium was used because it is a typical electrical contact for thin-film devices based on a-Si:H and μc-Si:H. In addition, the use of a metallic substrate leads to real-time spectra with $60° < \Delta < 120°$, and for this range, systematic errors are reduced in the rotating polarizer configuration.[13]

III. RESULTS AND DISCUSSION

In this study, we focus on the regime of μc-Si:H growth in which the film consists of isolated Si particles. In this case, a one-layer optical model for the film is a realistic approximation of the structure. In contrast, after the particles make contact, two layers are required in the optical model, representing the underlying "bulk" film and the remaining surface roughness layer generated in the nucleation process.[15]

In studies of discontinuous particle films, there are two sets of optical functions of interest. The first is the effective dielectric function (ϵ_1,ϵ_2) of the film that is measured directly and includes both the Si particles and intervening void volume. The second is the dielectric function of the particles themselves $(\epsilon_{1p},\epsilon_{2p})$ that can be inferred from (ϵ_1,ϵ_2) by mathematically eliminating the effect of the void-volume fraction using the EMT of Bruggeman in this case. In Secs. III A, III B, and III C, we describe the three-step sequence for determining the evolution of first (ϵ_1,ϵ_2), then the void-volume fraction, and finally $(\epsilon_{1p},\epsilon_{2p})$, respectively, from real-time spectra in (ψ,Δ) obtained during μc-Si:H particle film growth.

A. Evolution of the effective dielectric function

In order to determine the effective dielectric function (ϵ_1,ϵ_2) of the μc-Si:H film, we extract the correct physical thickness d, by trial and error, as the one that minimizes artifacts in (ϵ_1,ϵ_2) obtained by numerical inversion of (ψ,Δ).[16] Such artifacts arise from a feature in the Cr substrate dielectric function at 2.7 eV, and are introduced only when d is chosen incorrectly. An independent check of this method requires that the inverted ϵ_2 approach zero asymptotically at the lowest measurement energy of 1.5 eV.

Figure 1 shows effective dielectric functions (ϵ_1,ϵ_2) deduced by this approach for selected μc-Si:H film thicknesses over the range of $200 \le d \le 262$ Å. It should be kept in mind that since these spectra were collected during deposition, they are appropriate for a film temperature of 250 °C. We can point out a number of qualitative features in Fig. 1. First, the very low amplitudes of the dielectric functions are attributed to well-spaced Si particles with a very high intervening void-volume fraction. Second, the increasing amplitude with thickness reflects the reduction in void-volume fraction as the particles increase in size and approach one another. Third, the presence of the c-Si E_1 critical-point structure near 3.3 eV and the lack of any significant absorption strength from 2.0 to 2.5 eV, relative to that at 4 eV, show that the particles are, in fact, Si microcrystallites without a significant amorphous phase in the film. Buried beneath these dominant features in Fig. 1 are more subtle effects due to crystallite size. As we shall see in Sec. III C, the curvature in (ϵ_1,ϵ_2) near the E_1 critical point provides information on electron scattering at microcrystallite surfaces and how it is reduced as the crystallites increase in size.

Two considerations confine the analysis of the (ψ,Δ) spectra collected during growth to the relatively narrow range of film thickness in Fig. 1. First, for $d < 190$ Å, the void-volume fraction in the film is so high (>0.82, see Sec. III B) that the signal-to-noise ratio in (ϵ_1,ϵ_2) becomes unacceptable for the subsequent analysis described in Sec. III C. For $d > 265$ Å, the void fraction becomes small enough (~0.65) that a number of the closest microcrys-

tallites in the statistical distribution may make contact. If this occurs, then the association of crystallite size with physical thickness, expected to be valid in the regime of isolated nuclei, may begin to break down. Further comment on this possibility will appear at the end of Sec. III B.

B. Evolution of thickness and void-volume fraction

The next step in the analysis is to extract the evolution of the void-volume fraction from the (ϵ_1,ϵ_2) spectra versus time. We have employed two different approaches to do this, based on regression analysis. As the first approach, we adopt the procedure described earlier in which (ϵ_1,ϵ_2) is modeled with the Bruggeman EMT as a composite of *c*-Si and void. This approach neglects any possible finite-size effects in the *c*-Si component, but this inadequacy does not appear to invalidate the void-fraction determination.

In the second approach, we employ a highly simplified analytical expression for $(\epsilon_{1p},\epsilon_{2p})$ from the study of Aoki and Adachi,[17] chosen to fit (ϵ_1,ϵ_2) over the energy range $2 \leq h\nu \leq 3$ eV with an absolute minimum number of free parameters. The expression assumes that the dielectric function in this range is dominated by the onset of two-dimensional M_0 characteristic associated with the E_1 critical point (CP), namely,

$$\epsilon_p(h\nu) = -A_{a1}[\chi_{a1}(h\nu)]^{-2}\ln\{1-[\chi_{a1}(h\nu)]^2\} ,$$

where

$$\chi_{a1}(h\nu) = (h\nu + i\Gamma_{a1})/E_{a1} ,$$

and A_{a1}, E_{a1}, and Γ_{a1} are the amplitude, energy, and broadening parameter of the CP. We fix A_{a1} at the value obtained from the corresponding fit to the single-crystal dielectric function at 250 °C. Then the (ϵ_1,ϵ_2) spectra such as those of Fig. 1 are fit by regression analysis using three free parameters, E_{a1}, Γ_{a1}, f_v, the void-volume fraction. Typical results of the fitting procedure are shown in Fig. 1 (solid lines). Our confidence in the validity of the regression analyses for determination of the void-volume fraction is strengthened by the fact that f_v values obtained by the two completely independent approaches agree to within ± 0.01.

Although the second approach is an appropriate method for determining f_v, based on the reduction in the amplitude of (ϵ_1,ϵ_2) for the μc-Si:H film relative to bulk single-crystal Si, values of Γ_{a1} and E_{a1} are in error, as has been noted by inspection of the high-energy extrapolations of the fits (not shown). This problem results from neglecting other known important contributions to the analytical expression for the *c*-Si dielectric function over the $2 \leq h\nu \leq 3$ eV photon-energy range. These include the excitonic contribution from the E_1 CP and a contribution from the low-energy part of the E_2 CP,[17] both expected to be important at the higher energies of the fitted range, as well as contributions from indirect transitions, important at the lower energies. Thus, in such an analysis, we have no hope of deducing accurate information on the electronic structure directly from the effective dielectric function of the μc-Si:H because of the complexity of the physically meaningful model required to fit it.

Figure 2(a) shows the void fraction versus time during deposition obtained by regression analysis using the analytical expression for ϵ_p for thickness $190 < d < 320$ Å (open circles). The thicknesses obtained in the artifact minimization procedure of Sec. III A are also given in Fig. 2(a) (filled circles). When the thickness is fit to a linear relationship, the $d=0$ intercept occurs at $t=0$, indicating that the Si microcrystallites increase in size linearly, characterized by a physical thickness rate of 16 Å/min. For $d < 190$ Å, we assume that the values of d are given by the extrapolated rate (broken line); then (ϵ_1,ϵ_2) in this regime can be determined by mathematical inversion of the (ψ,Δ) spectra. Finally, these dielectric functions are fit by regression analysis using the first approach above, namely the EMT with a mixture of *c*-Si and void. The resulting void-volume fraction also appears in Fig. 2(a) (open triangles). The near continuity in f_v versus time in the region near $d=190$ Å ($t=11.75$ min), where the transition between the two modeling approaches is made, provides support for the validity of

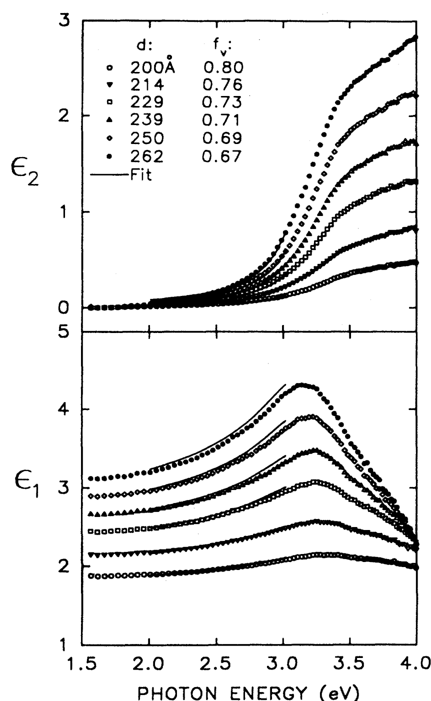

FIG. 1. Effective dielectric functions extracted from (ψ,Δ) spectra collected in real time during discontinuous μc-Si:H thin-film growth at selected times, identified by the physical thicknesses d, listed at the upper left. The substrate is an opaque layer of chromium on glass, held at 250 °C. A one-layer model was used for the film in order to extract d. The solid lines are three parameter fits to the effective dielectric function for $2 \leq h\nu \leq 3$ eV using a two-component version of the Bruggeman effective-medium theory. One component is *c*-Si, whose dielectric function is calculated from a simple analytical formula, and the other is void, whose volume fraction f_v is the free parameter of greatest interest here (listed alongside the corresponding thickness).

both. In Fig. 2(b), the mass thickness or Si volume per unit area, defined in our case by $d(1-f_v)$, is plotted using the combined results from the top panel of the figure.

The results of Fig. 2 in the earlier stage of the deposition can be understood on the basis of simple three-dimensional particle growth [see inset of Fig. 2(b)]. If the physical thickness is a linear function of time t and the particles are assumed to nucleate on a square grid with spacing s, then the mass thickness is given by $d_{\text{mass}}=(cr^3/s^2)t^3$. Here, r is the physical thickness rate (16 Å/min), and c is a unitless constant that depends on the particle shape (assumed to be unchanging over time). The expression $c=\pi\eta/6\gamma^2$ covers the simplest cases of spheroidal ($\eta=1$) and hemispheroidal ($\eta=4$) particles. In this expression $\gamma=d/b$ is the axial ratio of the spheroid, where b is the length of the major axis [parallel to the substrate plane; see inset Fig. 2(b)]. The solid line in Fig. 2(b) is the fit to this simple geometric model using results for $d<265$ Å to prevent potential biasing by microcrystallite contact. The void-fraction evolution corresponding to this fit, assuming the linear deposition rate, is given as the solid line in Fig. 2(a). Overall, the fits are quite good in the crystallite growth regime, considering the simplicity of the geometric model. The deviations in the observed d_{mass} from the cubic time dependence above 265 Å may result from the onset of partial crystallite aggregation. If the crystallites are assumed to be spherical, then the best fit provides a spacing of ~ 325 Å; for hemispherical crystallites, the spacing would be twice as large. The resulting range of possible nucleation densities for these two simple geometries, $(2-9)\times 10^{10}$ cm^{-2}, is a factor of 70–300 lower than that for *a*-Si:H on similarly prepared Cr substrates.

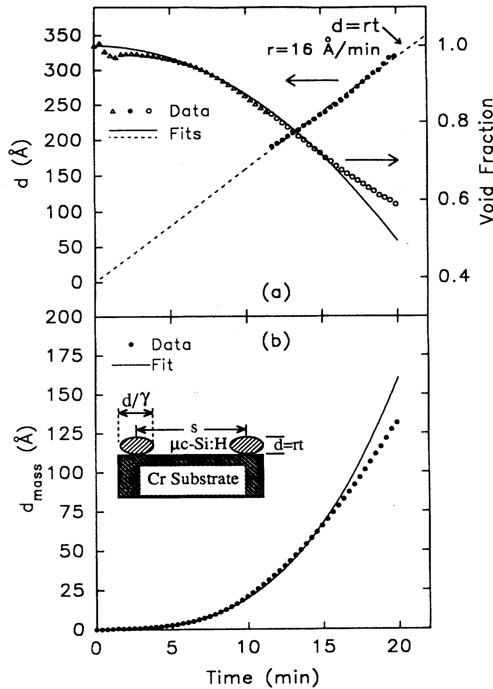

FIG. 2. Time evolution of the microstructure of the μc-Si:H film of Fig. 1, deduced from an analysis of (ψ,Δ) spectra collected in real time during growth. The physical thickness d (solid points) and the volume fraction f_v (open points) are presented in (a). The broken line is the best fit to d assuming a constant deposition rate r. The values of f_v denoted by open triangles were derived using the effective-medium theory and the single-crystal Si optical functions at 250 °C; for the open circles, an analytical formula for the *c*-Si optical functions was employed (see fits in Fig. 1). The mass thickness, or Si volume per unit area $d(1-f_v)$, is presented in (b). The solid line in (b) represents the best fit to the data, assuming three-dimensional, isolated particle growth, as shown schematically in the inset. The solid line in (a) is derived from the fit in (b) in accordance with $f_v=1-(d_{\text{mass}}/rt)$, where t is the elapsed time.

C. Evolution of the dielectric function of the Si microcrystals

Next, the void-volume fraction results in Fig. 2(a) can be used to extract the evolution of the dielectric function $(\epsilon_{1p},\epsilon_{2p})$ of the Si crystallites. These spectra are closely similar in shape to those in Fig. 1, but with significantly increased amplitudes. In order to characterize accurately the evolution of the electronic structure of the crystallites, we perform standard CP analysis on $(\epsilon_{1p},\epsilon_{2p})$. To be consistent with the study of Lautenschlager *et al.*[18] for bulk single-crystal Si, we assume a purely excitonic line shape for the E_1 critical point, i.e.,

$$d^2\epsilon_p/d(h\nu)^2=2A_{c1}\exp(i\phi_{c1})(h\nu-E_{c1}+i\Gamma_{c1})^{-3},$$

where A_{c1}, ϕ_{c1}, E_{c1}, and Γ_{c1} are the amplitude, phase, transition energy, and broadening parameter associated with the E_1 optical transitions. Figure 3 shows second-derivative spectra for single-crystal Si obtained on our multichannel ellipsometer with a measurement time and temperature of 3.8 s and 250 °C, respectively. In obtaining these results, we employ standard numerical routines for smoothing and differentiation. Although such an approach has been found to lead to systematic errors of ~ 0.01 eV in E_{c1} (Ref. 19), it is suitable for our purposes, given the intrinsically higher uncertainties in our data arising from the short acquisition time. Figure 3 also shows typical results for μc-Si:H at thicknesses of 191 and 250 Å derived from real-time observations. Significant broadening of the CP feature is observed in the Si microcrystallites in comparison to the single-crystal counterpart.

Figure 4 shows the transition energy, broadening parameter, and phase as a function of physical thickness from 190 to 250 Å. Error bars represent 90% confidence limits (defined by analogy to those of Ref. 7), determined from the regression analyses of the experimental second-derivative spectra. As noted earlier, we do not analyze data for later times in order to avoid the regime in which crystallites make contact. In addition, for earlier times there is insufficient material (i.e., $d_{\text{mass}}<35$ Å) to deduce $(\epsilon_{1p},\epsilon_{2p})$ spectra of the required quality for the CP-analysis differentiations. To obtain the results in the latter regime, a higher nucleation density would be required.

From Fig. 4, we find that the transition energy and phase associated with the critical point is constant with

thickness within our uncertainty due to systematic errors. Furthermore, the average values for these two parameters, $(E_{c1},\phi_{c1})=(3.26\ \text{eV}, -36°)$ [with a full data range of $(\Delta E_{c1},\Delta\phi_{c1})=(\pm 0.015\ \text{eV}, \pm 6°)$] are very close to the results obtained by Lautenschlager *et al.*[18] on static single-crystal Si at 250 °C, using a higher-precision, photomultiplier-based, serial-scanning ellipsometer $[(E_{c1},\phi_{c1})=(3.27\ \text{eV}, -40°)]$. The agreement in E_{c1} and ϕ_{c1} between this study and that of Ref. 18 provides support for the validity of our experimental results and CP analysis, in spite of the expected loss in statistical significance owing to the smoothing and differentiation procedures.

The broadening parameter in Fig. 4, on the other hand, decreases from 0.37 to 0.32 eV versus thickness, and is about a factor of 2 greater than that for single-crystal Si obtained either by us under the same measurement conditions (0.156 eV), or by Lautenschlager *et al.* (0.171 eV). As will be seen next, this behavior is to be expected for a finite-size effect in which electron scattering at microcrystallite surfaces limits the excited-state lifetime. However, the crystallites are large enough so that the nature and optical-transition energy of the CP are not altered.

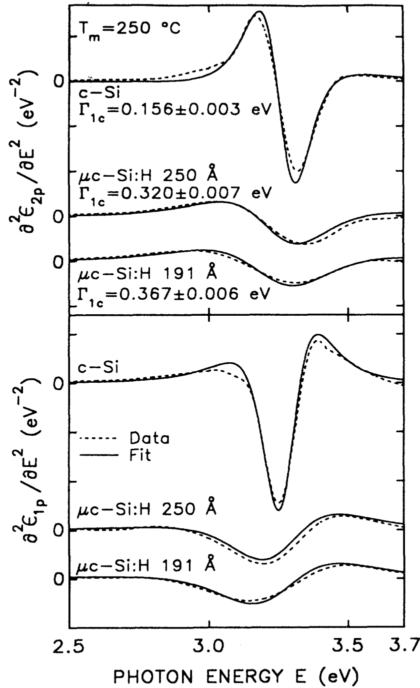

FIG. 3. Critical-point analyses applied to the E_1 transitions of the dielectric function for Si microcrystallites at physical thicknesses of 250 and 191 Å (lower curves). The critical-point amplitude, energy, broadening, and phase are determined from the fit (solid lines) to the second-derivative spectra (broken lines). Also shown are the corresponding results for bulk single-crystal Si (upper curves). The second derivatives are offset for clarity, and the ordinate is in units of 500 eV^{-2}. In all cases, the measurement temperature is 250 °C, and an excitonic line shape is assumed in accordance with Ref. 18.

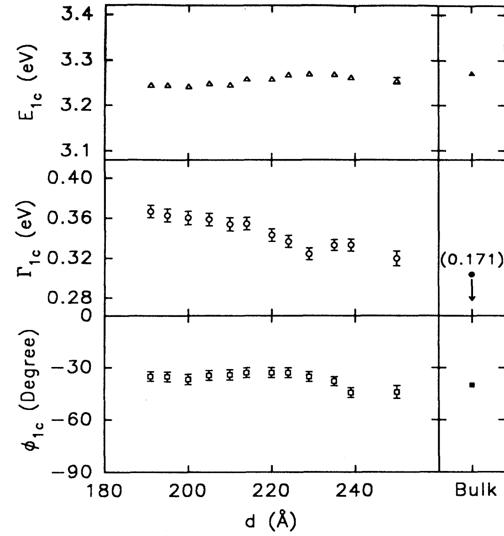

FIG. 4. Evolution of the electronic structure of the μc-Si:H thin film of Fig. 1 as a function of physical thickness at a measurement temperature of 250 °C. These results were obtained from fits such as those in Fig. 3. From top to bottom, the critical-point energy, broadening parameter, and phase are plotted, and values for single-crystal Si from the work of Ref. 18 at 250 °C are plotted at the far right. The broadening parameter for single-crystal Si from Ref. 18 is 0.171 eV. The error bars are the 90% confidence limits in the critical-point analysis.

The standard size-effect relationship is given by[20,21]

$$\Gamma_{c1}(d)=\Gamma_{c1,\text{bulk}}+h[v/\lambda(d)]\ , \tag{1}$$

where h is Planck's constant, $\lambda(d)$ is the mean free path, and v is the speed for electrons participating in the E_1 transitions, i.e., those with wave vector near the Λ point in the band structure. Here, all scattering mechanisms are assumed to be independent. We have included an explicit particle-diameter (or film thickness d) dependence in the mean free path, recognizing that the dominant mechanism may be scattering at particle surfaces that leads to the observed reduction in Γ_{c1} from $\Gamma_{c1,\text{bulk}}$, the single-crystal value. We can substitute $\lambda=d/2$ into Eq. (1) as long as isotropic surface scattering is the only mechanism and the particles are noncontacting and spherical.[21] If a number of particles make contact, then λ may increase, since the grain boundaries are expected to be less effective than surfaces in scattering electrons.

To assess the relevance of Eq. (1), in Fig. 5 we plot Γ_{c1} from the CP analysis versus d^{-1} for the set of data in Fig. 4. Roughly linear behavior is apparent, which is not unexpected, given the relatively narrow range in d^{-1}. However, the best-fit linear relationship extrapolates to within $\sim$0.01 eV of $\Gamma_{c1,\text{bulk}}$ from Ref. 18 at the $d\rightarrow\infty$ intercept, exactly as would be expected on the basis of Eq. (1). As another check of the model, the electron speed can be calculated from Fig. 5 as 4.7×10^7 cm/s. This is reasonable, given that the speed, $|\hbar^{-1}(dE/dk)|$, is 2.6×10^7 cm/s for electrons traveling in the $\langle 111\rangle$ direction with k at the Λ point, as calculated from the Si band structure.[22] Similar agreement has been obtained between the electron velocity estimated from the GaAs

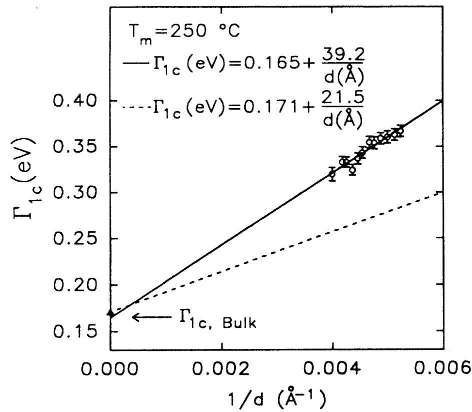

FIG. 5. Broadening parameter for the E_1 optical transitions of μc-Si:H at 250 °C, replotted from Fig. 4 as a function of inverse physical thickness (open points). The solid line is a linear fit to these results, suggesting agreement with a finite-size-effect theory, in accordance with Eq. (1). The triangular point is the broadening parameter for single-crystal Si at 250 °C (not included in the fit). The broken line is calculated from Eq. (1), assuming that the mean free path is $d/2$, the electron speed is 2.6×10^7 cm/s, and the bulk broadening parameter is 0.171 eV (Ref. 18).

band structure and that deduced experimentally from a size-effect analysis of a set of static μc-GaAs materials prepared from single-crystal GaAs by ion implantation.[23] The discrepancy in our case may arise from features not included in the analysis, such as a nonspherical microcrystallite shape, a distribution of sizes, or nondiffuse scattering at the surfaces. In general, we conclude that the film consists of high-quality Si crystallites; otherwise, defects internal to the crystallites would limit the electron lifetime and Γ_{c1} would include a crystallite size-independent contribution.

IV. SUMMARY

To summarize, real-time spectroscopic ellipsometry provides a comprehensive picture of the evolution of microstructure, optical properties, and electronic structure in microcrystalline silicon (μc-Si:H). The conversion of raw ellipsometric spectra expressed by (ψ,Δ) into physical information requires three major steps, outlined in Secs. III A–III C.

(1) First, the correct film thickness d is found by a trial-and-error procedure that results in the minimization of artifacts in the dielectric function of the μc-Si:H film, deduced by inversion from (ψ,Δ). The resulting dielectric functions (ϵ_1,ϵ_2), compared to those of single-crystal Si, indicate a significant void-volume fraction in the film to thicknesses of 300 Å, but no significant amorphous phase, under the film preparation conditions used here.

(2) The void-volume fraction f_v is established by an effective-medium theory whereby the dielectric function of the film is fit to an analytical form below the E_1 feature at 3.3 eV. Knowledge of the void fraction is important first because it allows us to calculate the evolution of the mass thickness d_{mass} or the volume of Si per unit area. In the initial ~250 Å in physical thickness, $d_{\text{mass}} \propto t^3$, where t is the elapsed time during deposition. This functional dependence is characteristic of three-dimensional growth of isolated particles. Second, the void fraction allows us to extract the dielectric functions of the microcrystallites themselves, $(\epsilon_{1p},\epsilon_{2p})$, from the effective dielectric functions of the growing film, (ϵ_1,ϵ_2).

(3) With the dielectric functions of the isolated Si microcrystallites ($d<250$ Å), we can perform a critical-point (CP) analysis of the E_1 optical transitions, to obtain the CP parameters characterizing the amplitude, transition energy, broadening, and phase. In our case, this is possible only over a relatively narrow range of thickness $190<d<250$ Å, owing to the very small volume of material at lower thicknesses ($d_{\text{mass}}<35$ Å), which reduces the quality of the deduced $(\epsilon_{1p},\epsilon_{2p})$. Over the accessible thickness range, however, the results are quite clear. Finite-size effects outside experimental uncertainties are observed only in the broadening parameter, and these can be readily accounted for by assuming that the excited-state lifetime for electrons is limited by scattering at Si crystallite surfaces. There is no indication that defects within the crystallites themselves play a role in the optical properties under the preparation conditions used here.

In concluding, we note that a reduction in the nucleation density results in a larger volume of material in the film for a given physical thickness. In theory, studies of the size effect can be extended to thinner films using this approach. In practice, higher nucleation densities are achieved with higher plasma powers, which generate substrate defects by high-energy particle impingement. Our initial experiences have shown that under such conditions, the resulting Si crystallites are also defective, but future efforts will be directed toward solving this problem and studying finite-size effects for smaller crystallites.

ACKNOWLEDGMENTS

This research was supported by the National Science Foundation under Grant No. DMR-8957159. One of us (R.W.C.) was also supported by the National Renewable Energy Laboratory under Subcontract No. XG-1-10063-10.

[1]For a collection of recent papers, see *Materials Issues in Microcrystalline Semiconductors,* edited by P. M. Fauchet, K. Tanaka, and C. C. Tsai, MRS Symposia Proceedings No. 164 (Materials Research Society, Pittsburgh, 1990).

[2]A. Matsuda, M. Matsumura, K. Nakagawa, T. Imura, H. Yamamoto, S. Yamasaki, H. Okushi, S. Iizima, and K. Tanaka, Jpn. J. Appl. Phys. **19**, L305 (1980).

[3]S. Guha, J. Yang, P. Nath, and M. Hack, Appl. Phys. Lett. **49**, 218 (1986).

[4]L. Genzel, in *Festkörperprobleme,* edited by H. J. Queisser (Vieweg, Braunschweig, 1974), Vol. XIV, p. 183.

[5]B. G. Bagley, D. E. Aspnes, A. C. Adams, and C. J. Mogab,

Appl. Phys. Lett. **38**, 56 (1981).
[6]R. W. Collins, W. J. Biter, A. H. Clark, and H. Windischmann, Thin Solid Films **129**, 127 (1985).
[7]D. E. Aspnes, Proc. Soc. Photo-Opt. Instrum. Eng. **276**, 188 (1981).
[8]G. E. Jellison, Jr., Appl. Opt. **30**, 3354 (1991).
[9]R. W. Collins, H. Windischmann, J. M. Cavese, and J. Gonzalez-Hernandez, J. Appl. Phys. **58**, 954 (1985).
[10]S. Logothetidis, J. Appl. Phys. **65**, 2422 (1989).
[11]M. Ingels, M. Stutzmann, and S. Zollner (Ref. 1), p. 229.
[12]I. An and R. W. Collins, Rev. Sci. Instrum. **62** , 1904 (1991).
[13]N. V. Nguyen, B. S. Pudliner, I. An, and R. W. Collins, J. Opt. Soc. Am. A **8**, 919 (1991).
[14]S. Usui and M. Kikuchi, J. Non-Cryst. Solids **34**, 1 (1979).
[15]I. An, H. V. Nguyen, N. V. Nguyen, and R. W. Collins, Phys. Rev. Lett. **65**, 2274 (1990).
[16]H. Arwin and D. E. Aspnes, Thin Solid Films **113**, 101 (1984).
[17]T. Aoki and S. Adachi, J. Appl. Phys. **69**, 1574 (1991).
[18]P. Lautenschlager, M. Garriga, L. Vina, and M. Cardona, Phys. Rev. B **36**, 4821 (1987).
[19]D. E. Aspnes, A. A. Studna, and E. Kinsbron, Phys. Rev. B **29**, 768 (1984).
[20]J. Euler, Z. Phys. **137**, 318 (1954).
[21]U. Kreibig, J. Phys. F **4**, 999 (1974).
[22]J. R. Chelikowsky and M. L. Cohen, Phys. Rev. B **14**, 556 (1976).
[23]G. F. Feng and R. Zallen, Phys. Rev. B **40**, 1064 (1989).